Considerations on using single electron scattering on tungsten, for the calibration of the HPS ECal

Luca Colaneri Supervisor: Annalisa D'Angelo

March 24, 2014

1 Single electron scattering kinematics

For ultrarealativistic electrons $E \gg mc^2$ and $E \approx |\mathbf{p}|$ and the following approximation applies for the elastically scattered electron energy E' from a nucleus in the laboratory system:

$$E' = \frac{E}{1 + \frac{E}{M}(1 - cos\theta)} \tag{1}$$

where E is the beam energy, M is the target mass and θ is the scattering angle.
Considering the HPS set up and a tungsten target, we may set $M = 171.24$ GeV and plot the scattered electron energy E' VS the scattering angle θ, within the ECal geometrical acceptance ($\Delta\theta < 300$ mrad), for different values of the beam energy E, obtaining the curves shown in Figure 1.

The expected ECal energy resolution, according to the HPS proposal, is $\frac{4\%}{\sqrt{E}}$, which corresponds to $\delta E \approx 30\ MeV$, $\delta E \approx 20\ MeV$ and $\delta E \approx 6\ MeV$, for incoming electron energies equal to $E = 1.5\ GeV$, $E = 2.2\ GeV$ and $E = 6.6\ GeV$, respectively, as summarized in Table 1. The energy variation $\Delta E'$ of the scattered electrons within ECal is negligible at lower energies, but not at $E = 6.6\ GeV$.

Beam Energy (GeV)	Ecal resolution δE (MeV)	$\Delta E'$ (MeV)
1.5	30	0.7
2.2	20	1.4
6.6	6	14

Table 1: Expected energy resolution of ECal compared with scattered electrons energy spread within ECal acceptance at different beam energies

2   Elastic Electron Scattering Cross Section

The elastic scattering cross section may be computed starting from the Mott cross section, taking into account the electric form factor for the tungsten target:

$$\frac{d\sigma}{d\Omega}(E,\theta) = \frac{(Ze^2)^2}{(4\pi\epsilon_0)^2 4E^2 \sin^4 \frac{\theta}{2}}(1-\beta^2\sin^2\frac{\theta}{2})|F(Q)|^2 \tag{2}$$

where:

$$F(Q) = \frac{3}{(QR)^3}(\sin(QR) - QR\cos(QR)) \tag{3}$$

with $Q^2 = -(P-P')^2$, $Q = \sqrt{Q^2} \approx |\vec{p}|$ being the transferred four-momentum and R the nucleus radius, given by $R = 1.21 fm A^{\frac{1}{3}}$. For a tungsten target we have $A \approx 183$ and $Z = 74$. Writing the magnetic permeability of vacuum ϵ_0 as:

$$\epsilon_0 = \frac{e^2}{2\alpha hc} = \frac{e^2}{2\alpha 2\pi\hbar c} \tag{4}$$

and using natural units:

$$\epsilon_0 = \frac{e^2}{4\pi\alpha} \text{ or } \alpha = \frac{e^2}{4\pi\epsilon_0} \tag{5}$$

the differential cross section then reads:

$$\frac{d\sigma}{d\Omega} = \frac{Z^2\alpha^2(1-\beta^2\sin^2\frac{\theta}{2})}{4E^2\sin^4\frac{\theta}{2}}\left(\frac{3}{(QR)^3}(\sin(QR) - QR\cos(QR))\right)^2 \tag{6}$$

Figure 2 shows the plots of the differential cross section as a function of the electron scattering angle in the ECal acceptance range, for electron beam energies $E = 1.5\ GeV$ (top), $E = 2.2\ GeV$ (middle) and $E = 6.6\ GeV$ (bottom).

The graphs show a rapid drop of the differential cross section of several orders of magnitude, within the ECal acceptance, for larger scattering angles; this effect is more dramatic as the beam energy increases. We expect a lot more events in the central region of the calorimeter than in the borders. At 6.6 GeV the drop of counts becomes critical.

3   Integrated cross sections

We want to estimate the number of elastic electron scattering events that would be detected by each ECal crystal. The rates are calculated according to the following expression:

$$\frac{dN_{E'}}{dt} = \frac{I_e}{q_e}\frac{\rho \cdot N_{av} \cdot l}{A}\Delta\sigma \tag{7}$$

2

where $\frac{dN_{E'}}{dt}$ is the number of scattered electrons per unit of time, $I_e = 200\ nA$ is the beam current, $q_e = 1.6\ 10^{-19}C$ is the electron charge, $\rho = 19,3\ \frac{gm}{cm^3}$ is the tungsten density, $N_{av} = 6.022\ 10^{23}(gm^{-1})$ is the Avogadro number, equal to the inverse of atomic mass unit expressed in grams, $l = 5\mu m$ is the target thickness, $A = 183.35$ is the average tungsten atomic number for natural isotope composition and $\Delta\sigma$ is the differential cross section from equation (6) integrated over the acceptance of a single ECal crystal.

Substituting all numbers one obtains:

$$\frac{dN_{E'}}{dt} = \mathbb{L}\Delta\sigma = 3.95\ 10^{31}\ cm^{-2}s^{-1}\Delta\sigma \tag{8}$$

and

$$\frac{dN_{E'}}{dt} = \mathbb{L}\Delta\sigma = 8.93\ 10^{31}\ cm^{-2}s^{-1}\Delta\sigma \tag{9}$$

where the values of the luminosity $\mathbb{L} = 3.95\ 10^{31}\ cm^{-2}s^{-1}$ and $\mathbb{L} = 8.93\ 10^{31}\ cm^{-2}s^{-1}$ have been obtained. The integration of the cross section (6) over each single ECal crystal geometrical acceptance would require the change of variables from polar to Cartesian ones, which is not straight forward. The following geometrical and mathematical simplifications have been performed to calculate $\Delta\sigma$. The cross section depends on the polar electron scattering angle θ while it is independent from the azimuthal angle ϕ; therefore the ECal geometry has been divided into five sectors corresponding to fixed intervals of θ, according to Figure 3, where the upper left quadrant of the ECal is shown. The other quadrants are obtained applying symmetry considerations and identical numbers are obtained.

The following geometrical dimensions have been considered:

- L=34 cm (half-calorimeter widh)

- h= 4 cm (distance of the bottom of the ECal quadrant from the x-z plane equal to half of the ECal vertical opening)

- H=6.5 cm (half of calorimenter height = 1.3 cm x 5 crystals)

- d=139.7 cm (distance of the calorimeter face from the target)

- r = $d\tan(\theta)$ (radial distance of the crystals from the beam axis)

For each sector a maximum and a minimum value of both the polar angle θ and the azimuthal angle ϕ have been identified, over which the differential cross section (6) may be averaged and integrated. Table 3 shows the intervals of the the polar angles θ and the variation of the corresponding azimuthal angles ϕ as a function of θ (and r), for each of the five sectors.

The first sector has been chosen to cover all ϕ angles from the minimum value $arcsin(\frac{h}{r})$ to 90° and corresponds to a polar aperture of $\Delta\theta = 0.46\ mrad$. The following three sectors have been obtained dividing the residual values of the ECal acceptance into three equal

3

sector number	$\theta_{min}(mrad)$	θ_{max} (mrad)	$\Delta\theta$ (mrad)	ϕ_{min}	ϕ_{max}
sector 1	28	74.31	46.31	$arcsin(\frac{h}{r})$	$\pi/2;$
sector 2	74.31	129.64	55	$arcsin(\frac{h}{r})$	$arcsin(\frac{h+H}{r})$
sector 3	129.64	184.98	55	$arcsin(\frac{h}{r})$	$arcsin(\frac{h+H}{r})$
sector 4	184.93	240.32	55	$arcsin(\frac{h}{r})$	$arcsin(\frac{h+H}{r})$
sector 5	240.32	249	8.68	$arccos(\frac{L}{r})$	$arcsin(\frac{h+H}{r})$

Table 2: Intervals of the polar (θ) and azimuthal (ϕ) angles corresponding to the five sectors shown in Figure 3.

intervals of $\Delta\theta = 0.55\ mrad$. The last sector corresponds to the residual, most distant, ECal corner.

The following formula for the numerical integration over all crystal of each sector, has been used:

$$\sigma_n = \sum_{i=1}^{1000} \frac{d\sigma(\theta_i, E)}{d\Omega} sin\theta_i \left(\phi_{max}(\theta_i, n) - \phi_{min}(\theta_i, n)\right) \Delta\theta_i = \sum_{i=1}^{1000} \delta\sigma_i(E, \theta_i, n) \qquad (10)$$

where n is the geometrical sector number $n = 1, .., 5$; σ_n is the integrated cross section over each of the five geometrical sectors; $\frac{d\sigma(\theta_i)}{d\Omega}$ is the differential cross section from equation (6) for a fixed beam energy E and scattering angle θ_i; θ_i assumes values from $\theta_{min}(mrad)$ to θ_{max}, in steps of $\Delta\theta_i = \frac{\Delta\theta}{1000}$ (mrad) for each sector, according to Table 3; $\phi_{max}(\theta_i, n)$ and $\phi_{min}(\theta_i, n)$, are the maximum and minimum values of the azimuthal angles, covered by each sector n of the ECal, as a function of the scattering angle θ_i.

Figures 4, 5 and 6 show plots of the dependence of each element of the sum $\delta\sigma_i(E, \theta_i, n)$ of equation (11) over the scattering angles θ_i, for each of the five sectors and for three different beam energies: $E = 1.5$ GeV, $E = 2.2$ GeV and $E = 6.6$ GeV, respectively.

The effect of the minima in the differential cross section, due to the existence of zeros in the electric form factor, is visible in Figure 6 at $E = 6.6$ GeV.

The numerical values for the cross sections σ_n, integrated over all the crystals of each sector, are shown in Table 3. We may notice that the cross sections drop of some orders of magnitude increasing the electron energy, in the same sector, as expected. In the approximation where we average over the cross section variation within each sector (which is valid at approximately a 10% level), we may divide the total cross section over each sector σ_n by the number N of crystals in each sector to obtain the average integrated cross section over one crystal acceptance $\Delta\sigma$, for each sector.

$$\Delta\sigma_n = \frac{\sigma_n}{N} \qquad (11)$$

The corresponding values are listed in of in Table 4.

4

E_{beam} (GeV)	σ_1 (mb)	σ_2(mb)	σ_3 (μb)	σ_4(μb)	σ_5 (nb)
1.5	70	7	663	125	663
2.2	31	3	191	21	191
6.6	2	0.02	0.273	0.008	0.410

Table 3: Numerical values of the cross sections σ_n,integrated over all the crystals of each sector.

E_{beam} (GeV)	$\Delta\sigma_1$ (mb)	$\Delta\sigma_2$(μb)	$\Delta\sigma_3$ (μb)	$\Delta\sigma_4$(nb)	$\Delta\sigma_5$ (nb)
1.5	2.91	200	x 20.09	3210	221
2.2	1.29	85.7	5.787	538	63.666
6.6	0.083	0.571	$8.27 \cdot 10^{-3}$	0.205	0.136

Table 4: Average integrated cross sections over the single crystal acceptance, for each sector.

Introducing the values of Table 4 into equation (7) we obtain the rate of expected hits per crystals in the five different angular sectors for each beam energy, as reported in Table5.

It may be noticed quite a high rate is available at all energies in the first sector, while this value drops of about one order of magnitude moving to the next angular sector for a fixed beam energy. Another reduction of at least one order of magnitude is observed, increasing the beam energy for a fixed sector. The overall variation over a factor of one million occurs across the different crystals of the ECal, at different energies. In particular the use of elastic scattering events seems not possible for the calibration of the crystals in the three more external sectors for a beam energy of $E = 6.6$ GeV.

E (GeV)	$\frac{dN}{dt}(s^{-1})$ sector 1	$\frac{dN}{dt}(s^{-1})$ sector 2	$\frac{dN}{dt}(s^{-1})$ sector 3	$\frac{dN}{dt}(s^{-1})$ sector 4	$\frac{dN}{dt}(s^{-1})$ sector 5
1.5	$116 \cdot 10^3$	$7.9 \cdot 10^3$	799	127	9
2.2	$5.2 \cdot 10^4$	$3.1 \cdot 10^3$	$2.3 \cdot 10^2$	21.6	2.5
6.6	$6.9 \cdot 10^3$	50	0.73	$1.9 \cdot 10^{-2}$	1.2×10^{-2}

Table 5: Expected average number of hits per unit of time for each crystal in the five angular sectors, shown in Figure 3, for three different beam energies E

4 Summary and Conclusions

At low beam energies, the electrons are elastically scattered practically at the same energy, regardless of the scattering angle, within the ECal acceptance. At 6.6 GeV, the energy differences become of the same order of the requested energy resolution, therefore the angular position of the absorbed scattered electron energy must be taken into account when defining a the calibration plan.
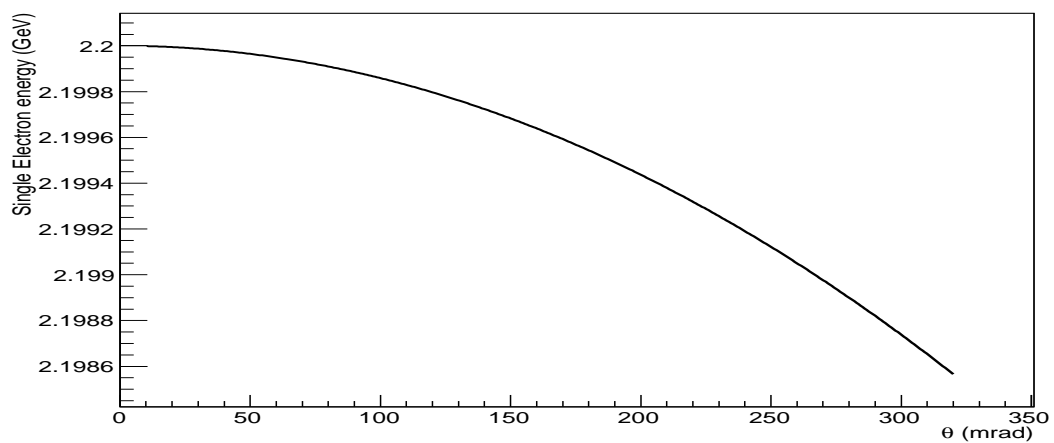
The differential cross sections of single electrons scattered off tungsten nuclei have been plotted. An approximate integration over the geometric acceptance of single crystals of the ECal has been performed, in order to calculate the effective number of events at a given luminosity, as a function of the crystal position. At 6.6 GeV the effect of the electric form factor becomes relevant, lowering by several orders of magnitude the cross section at larger angles. The use of the elastic scattered electrons events seems possible at lower beam energies $E = 1.5$ GeV and $E = 2.2$ GeV, while events rate critically drops at $E = 6.6$ GeV for the outer sectors of ECal.

Figure 1: Scattered electron energy (GeV) VS scattering angle (mrad)

Coulomb scattered electron energy (Beam Energy=1.5 GeV)
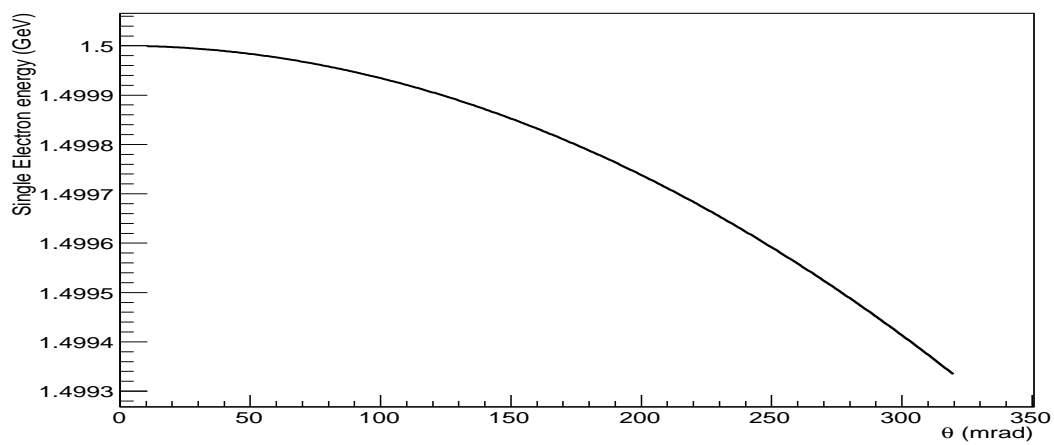
Coulomb scattered electron energy (Beam Energy=2.2 GeV)

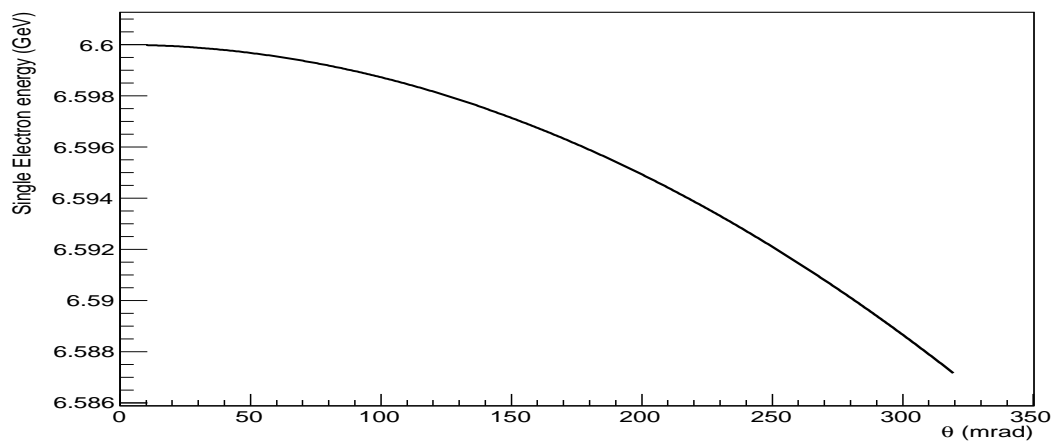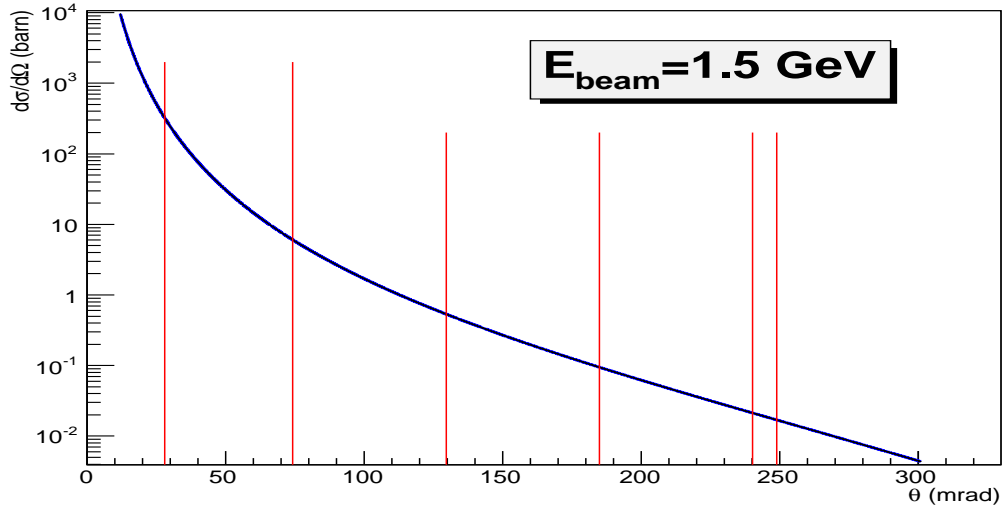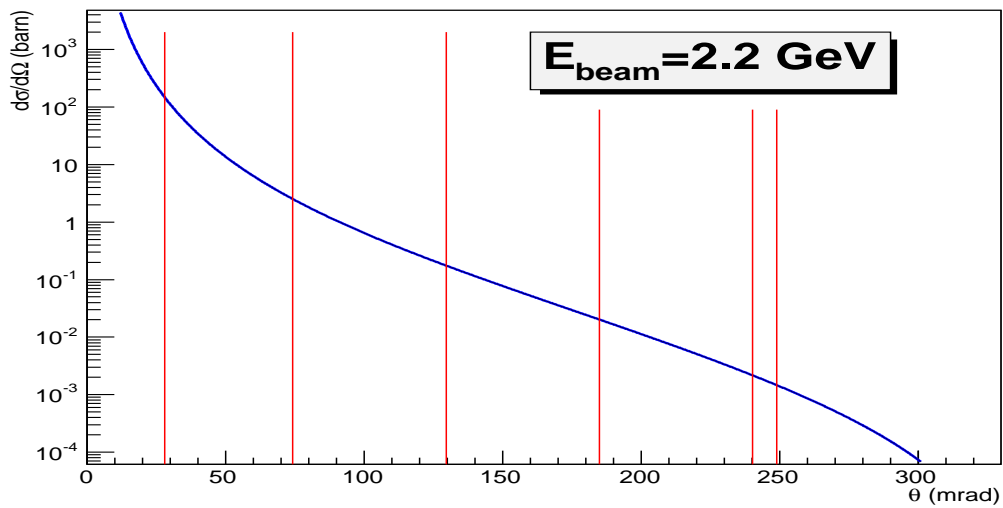Coulomb scattered electron energy (Beam Energy=6.6 GeV)

Figure 2: Differential cross sections of electron scattering off tungsten nucleus. Vertical red lines define the angular spread corresponding to each of the sectors defined in Figure3
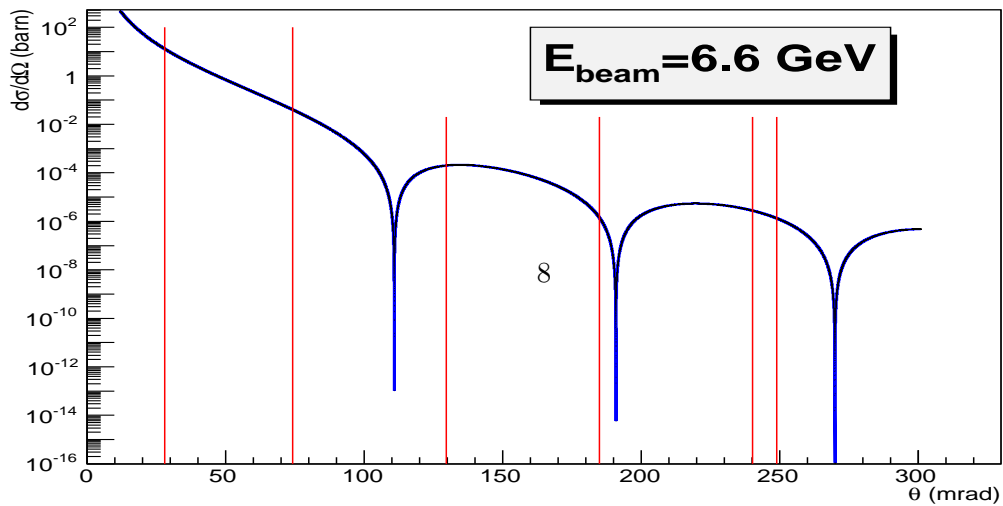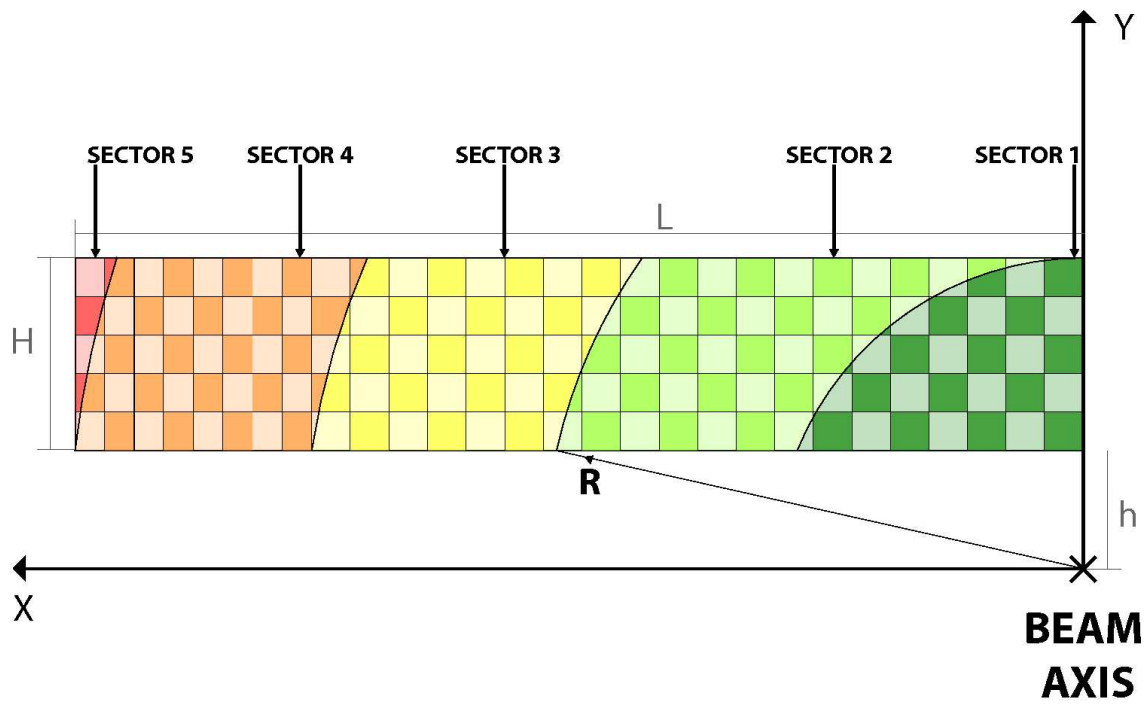

8

Figure 3: The upper-left face of the calorimeter showing the crystal granularity and divided into five sectors of fixed polar angle intervals.

Figure 4: Dependence of each element of the sum $\delta\sigma_i(E, \theta_i, n)$ of equation (11) from the scattering angles θ_i at E_{beam}=1.5 GeV
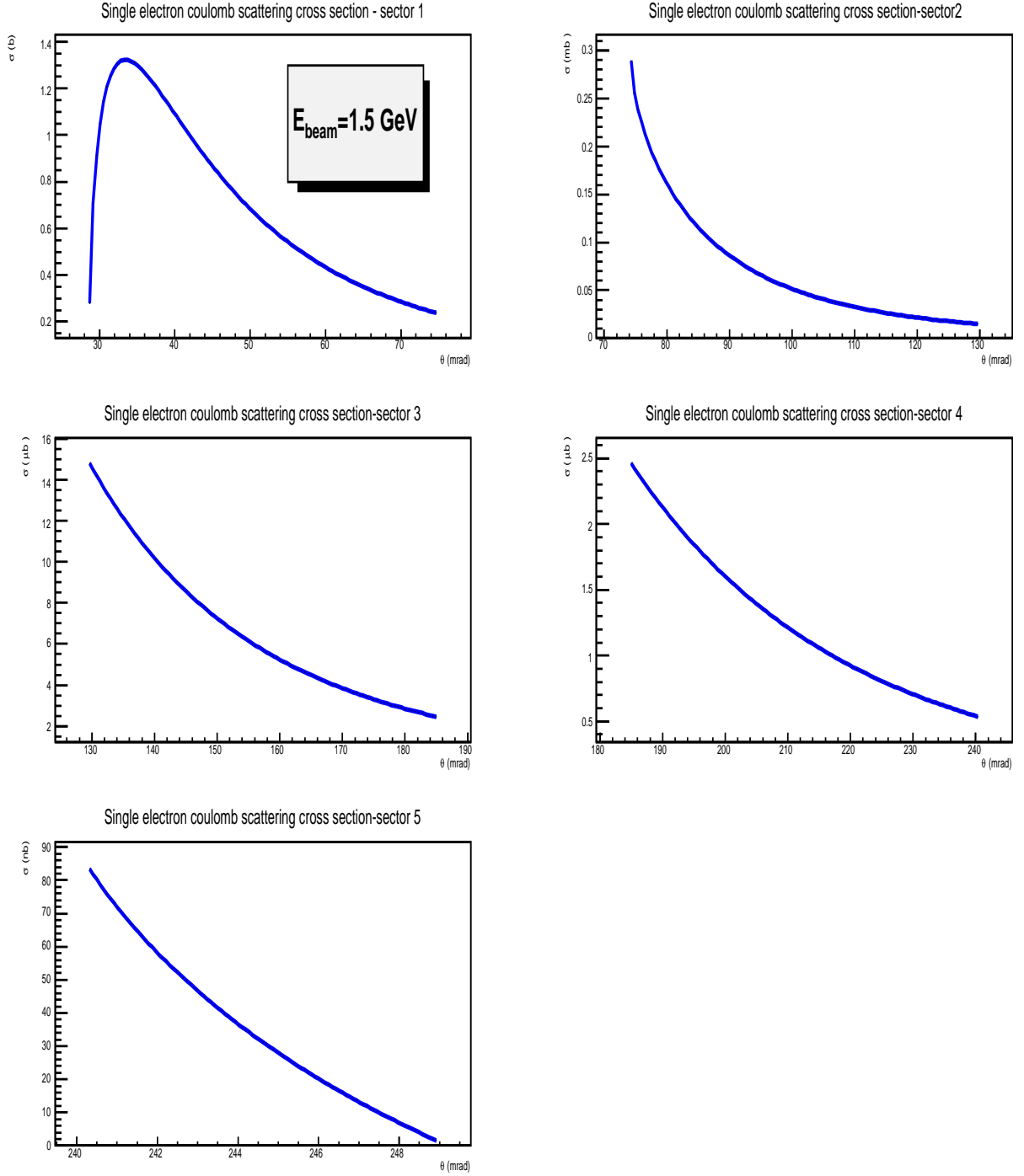

10

Figure 5: Dependence of each element of the sum $\delta\sigma_i(E, \theta_i, n)$ of equation (11) from the scattering angles θ_i at E_{beam}=2.2 GeV

Single electron coulomb scattering cross section - sector 1

E_{beam}=2.2 GeV

Single electron coulomb scattering cross section-sector2

Single electron coulomb scattering cross section-sector 3

Single electron coulomb scattering cross section-sector 4

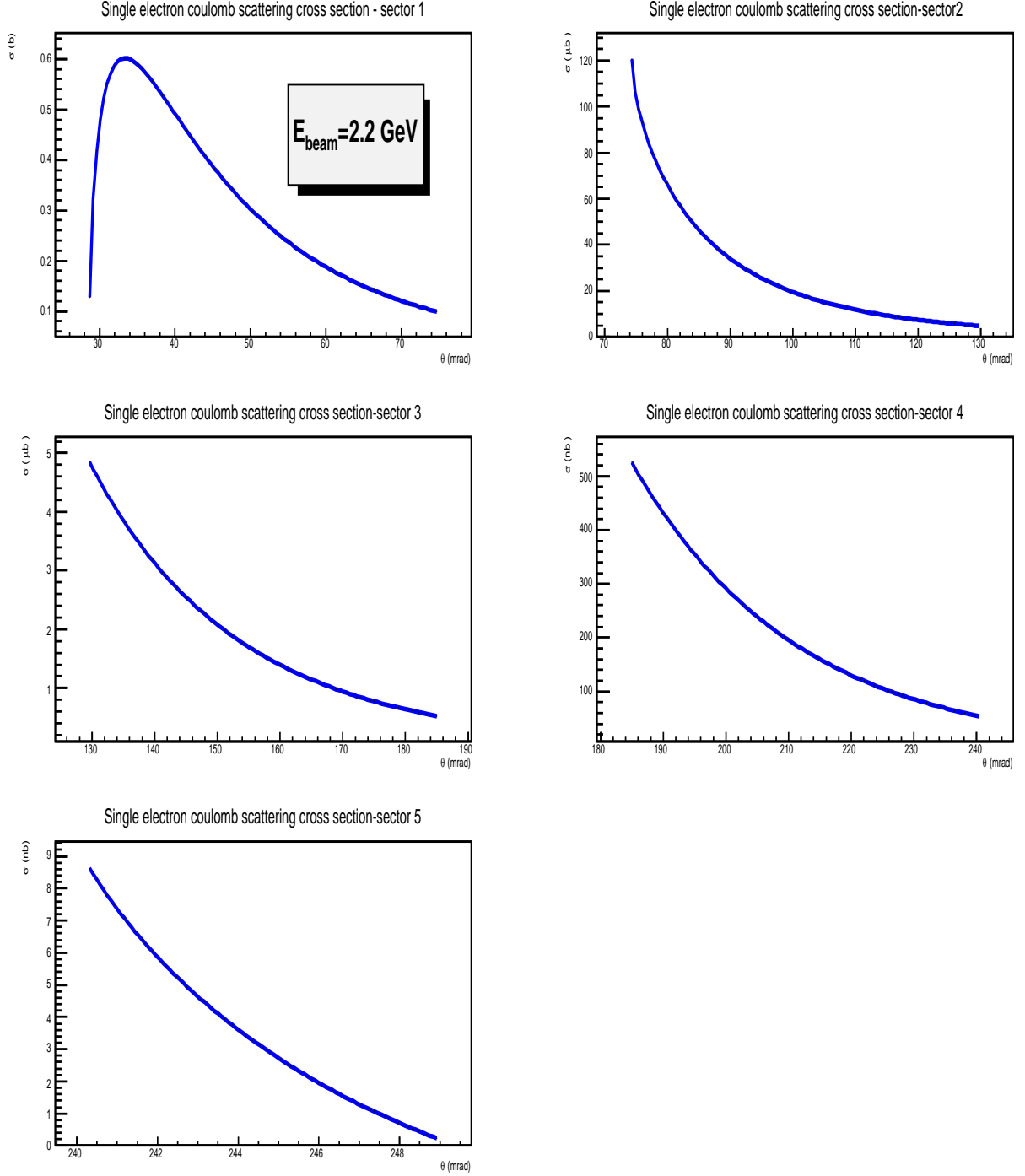
Single electron coulomb scattering cross section-sector 5

Figure 6: Dependence of each element of the sum $\delta\sigma_i(E, \theta_i, n)$ of equation (11) from the scattering angles θ_i at E_{beam}=6.6 GeV